Journal of Structural Engineering. Submitted May 4, 2012; accepted November 28, 2012;
posted ahead of print December 1, 2012. doi:10.1061/(ASCE)ST.1943-541X.0000781

Monitoring Crack Propagation in Reinforced Concrete Shear Walls by Acoustic Emission

Alireza Farhidzadeh[1], Ehsan Dehghan-Niri[2], Salvatore Salamone[3*], Bismarck Luna[4], Andrew Whittaker[5]

ABSTRACT

In the last two decades, several efforts have been made to monitor the cracking behavior in reinforced concrete (RC) structures. A technique that shows promise is Acoustic Emission (AE). This paper presents the results of an experimental study aimed at monitoring fracture processes in a large-scale RC shear wall using one of the most important AE parameters, that is, the *b*-value. The specimen was subjected to a displacement controlled reversed cyclic loading. A Gaussian filter is proposed to improve the interpretation of *b*-value data obtained during the test. In addition, a cluster analysis based on the *k*-means is presented to automatically classify the signal into tensile and shear cluster. Finally, a new algorithm called Sifted *b*-value (S*b*) analysis

[1] S.M.ASCE, Ph.D. Candidate, *Smart Structures Research Laboratory (SSRL), Department of Civil, Structural and Environmental Engineering, University at Buffalo, State University of New York, 212 Ketter Hall, Buffalo, NY, 14260 Email:alirezaf@buffalo.edu*

[2] S.M.ASCE, Ph.D. Candidate, *Smart Structures Research Laboratory (SSRL), Department of Civil, Structural and Environmental Engineering, University at Buffalo, State University of New York, 212 Ketter Hall, Buffalo, NY, 14260 Email:ehsandeh@buffalo.edu*

[3*] M.ASCE, Assistant Professor, Director *Smart Structures Research Laboratory (SSRL), Department of Civil, Structural and Environmental Engineering, University at Buffalo, State University of New York, 212 Ketter Hall, Buffalo, NY, 14260;* Email: *ssalamon@buffalo.edu;* Tel: +1(716)645-1523; Fax: +1(716) 645-3667; corresponding author

[4] S.M.ASCE, Ph.D. Candidate, *Department of Civil, Structural and Environmental Engineering, University at Buffalo, State University of New York, 212 Ketter Hall, Buffalo, NY, 14260, Email: bismarck@buffalo.edu*

[5] S.E. ASCE, Professor and Chair, *Department of Civil, Structural and Environmental Engineering, University at Buffalo, State University of New York, 212 Ketter Hall, Buffalo, NY, 14260, Email: awhittak@buffalo.edu*

Journal of Structural Engineering. Submitted May 4, 2012; accepted November 28, 2012;
posted ahead of print December 1, 2012. doi:10.1061/(ASCE)ST.1943-541X.0000781

is introduced to monitor the evolution of each crack mode. The proposed approach is capable to identify the initial yielding and eventually provide an early warning for the planning and implementation of remedial action to the structure at a point where it is less expensive and invasive than when its structural performance has been seriously compromised.

Subject Headings: Acoustic Emission, Sifted *b*-value analysis, Crack classification, *k*-means, Reinforced Concrete Shear Wall.

INTRODUCTION

Reinforced Concrete shear walls (RCSW) are widely used in conventional building and safety-related nuclear structures. They provide much or all of a structure's lateral strength and stiffness to resist earthquake and wind loadings. The cracking behavior of these critical structural elements is crucial due to its harmful effects on structural performance such as serviceability and durability requirements. Currently, the vast majority of inspections are visual, and unfortunately, even with the recent advances in automated ground-based nondestructive evaluation (NDE) methods, there is a potential that indications of structural degradation could be missed. In the past two decades, significant efforts have been made toward the development of structural health monitoring (SHM) systems in order to reduce life-cycle costs and improve the safety of civil infrastructures. A technique that shows promise for monitoring RC structures is Acoustic Emission (AE). In general, AE are stress waves caused by sudden strain releases due to internal fracture such as concrete cracking (Grosse and Ohtsu, 2008). When a material is overstressed, a burst of energy is released in the form of high frequency sound waves from propagating cracks or from plastic deformation. Characterizing the nature of AE sources is an open discussion in the

Journal of Structural Engineering. Submitted May 4, 2012; accepted November 28, 2012;
posted ahead of print December 1, 2012. doi:10.1061/(ASCE)ST.1943-541X.0000781

scientific literature due to the complexity of the AE signals. They are affected by several factors, including: 1) characteristics of the source; 2) the path taken from the source to the sensor; 3) the sensor's characteristics; and 4) the measuring system (Holford and Lark, 2005; Miller and Hill, 2005). Statistical-based pattern recognition algorithms have been proposed to automatically recognize and classify AE sources (Farhidzadeh et al., 2012; Godin et al., 2005; Godin, 2004; Kostopoulos, 2003; Manson et al., 2001; Pappas et al., 1998; Salamone et al., 2011; Aggelis, 2011). In general, some relevant features are extracted from the AE signals to characterize the source of the AE as well as to perform the critical tasks of detection, location and determination of the behavior of cracks that are likely to cause serious impairment of the structure and its ability to perform as designed. Extracting features from the AE signal is usually referred to as a parameter-based technique. Figure 1 shows a typical AE signal with the most common features used during an AE testing (i.e., peak amplitude, rise-time, duration, and count). A threshold is set somewhat above the background level and serves as a reference for the waveform features. The AE peak amplitude is defined at the maximum amplitude of the signal. The number of times the signal rises and crosses the threshold is the count of the AE event. The time period between the rising edge of the first count and the falling edge of the last count is the duration of the AE event. Finally, the time period between the rising edge of the first count and the peak of the AE event is defined to be the rise time.

In a previous study conducted by the authors on a shear wall with aspect ratio equal to 0.54 (Farhidzadeh et. al 2012), a classical *b*-value analysis has been carried out to monitor the fracture process during multiple load cycles of increasing magnitude. It has been shown that the classical approach cannot produce conclusive results. In addition**,** a statistical algorithm based on an

Journal of Structural Engineering. Submitted May 4, 2012; accepted November 28, 2012;
posted ahead of print December 1, 2012. doi:10.1061/(ASCE)ST.1943-541X.0000781

outlier analysis has been proposed to automatically identify the moment of yielding of the specimen. In this paper, three main novelties are proposed based : 1) a Gaussian filter to improve the interpretation of the *b*-value data, 2) a cluster analysis, based on the *k*-mean, to automatically classify the two fundamental crack modes (i.e., tensile and shear) and 3) an algorithm called "Sifted *b*-value (S*b*) analysis" to track the micro-to-macro crack transition stages for each crack mode. In fact, since the dominancy of shear class can be used as an early alarm, imminent failure can be prevented by selecting an appropriate rehabilitation scenario (Paterson 2001; Priestley and Seible 1996; Zhou and Attard 2012). The proposed algorithms have been validated during the experimental testing of a large scale RC shear wall with aspect ratio of 0.94.

This paper is organized as follows. The next section provides a brief overview of the *b*-value analysis, including a description of the Gaussian filter used to improve the interpretation of the results. A cluster analysis based on the *k*-means analysis is presented to perform crack classification. The new algorithm called "Sifted *b*-value" is then proposed to correlate b-value analysis with cluster analysis. The following sections describes the experimental investigation and the results. Finally conclusions are summarized.

b-VALUE ANALYSIS

The similarity between AE generated by materials undergoing brittle failure and seismic waves generated by earthquakes encouraged the use of seismological techniques such as the *b*-value analysis in AE applications (Gutenberg and Richter, 1949; Hardy, 1972). The *b*-value is obtained using frequency–magnitude distribution data by means of the Gutenberg–Richter relationship, which is generally used in seismology. The Gutenberg–Richter equation for AE is defined as

Journal of Structural Engineering. Submitted May 4, 2012; accepted November 28, 2012;
posted ahead of print December 1, 2012. doi:10.1061/(ASCE)ST.1943-541X.0000781

follows:

$$logN = a - b\left(\frac{A_{dB}}{20}\right) \quad (1)$$

where N is the incremental frequency (i.e., the number of AE signals with amplitude greater than A_{dB}), a and b are both empirical constants to be estimated from the linear curve fitting. a is the intercept of the line with $logN$ axis, b (which is called b–value) is the slope, and A_{dB} is the peak amplitude of the AE signal in decibels. The denominator of 20 is a scale factor due to the calculation of AE amplitude in dB; while in the original Gutenberg-Richter equation, the earthquake magnitude is proportional to the logarithm of the maximum amplitude. The factor of 20 is typically applied so that the estimated values are in the range as b-values observed from earthquakes, i.e. this is only a matter of scaling and nothing more. The b-value analysis of the AE signals is, in general, applied to a certain number n of AE signals. Suggested values of n found in the literature range from 50 to 100 (Shiotani et al., 2001). Several studies have shown that during the process of fracture of a RC specimen, there is a relationship between the b-value and the types of cracks. In general, the b-value increases during the formation of micro-cracks (i.e., early stages of damage) and decreases when the macro-cracks begin to localize (Colombo et al., 2003). Kurz (2006) used the b-value and the improved b-value (Ib) (Shiotani et al., 2001) on concrete specimens to connect stress redistribution to b-value drop and macro-crack formation during the fracture process. A minimum b-value analysis is demonstrated to be capable of estimating the load capacity of bridge girders (Schumacher et al., 2010). Experimental studies have also been performed to recognize defect size distributions in concrete structures (Carpinteri et al., 2007). The feasibility of micro-crack identification under compression and investigation of the fracture process in concrete made of recycled aggregate have also been demonstrated

Journal of Structural Engineering. Submitted May 4, 2012; accepted November 28, 2012;
posted ahead of print December 1, 2012. doi:10.1061/(ASCE)ST.1943-541X.0000781

(Watanabe et al., 2007). Although AE methods based on *b*-value analysis show promise in monitoring the behavior of cracks in small scale RC specimens, only a few if any such methods have been transitioned to field applications. A reason for this lack of acceptance are the large fluctuations of the *b*-value caused by normal operating conditions of the structure (e.g., temperature variations), which makes interpreting the results extremely difficult (Farhidzadeh et al., 2012). In this paper, a Gaussian filter is proposed to overcome this limitation.

Gaussian Filters

Gaussian filters are often used to smooth a signal before extracting primary features. Gaussian functions have the following properties that make them particularly useful in smoothing filters (Lin et al., 1996): 1) the Gaussian function is symmetric about the mean, and the weights assigned to signal values decrease gradually with distance from the mean; 2) the width of the Gaussian function is determined by its spread parameter, i.e., the standard deviation. As the standard deviation decreases, the Gaussian function does less smoothing; on the contrary, as the spread parameter increases, the amount of smoothing is increased. 3) The local extrema (e.g., *b*-value drop caused by overloads) observed at one standard deviation is also observable at the smaller standard deviations and no additional local extrema are created as the spread parameter increases. This property is important when analyzing the change of local extrema across different spread parameters. The first problem in Gaussian smoothing is how to determine the spread parameter for smoothing a given vector (or time waveform). It has been shown that there is no single value of standard deviation which is universally correct (Witkin, 1984; Yuille and Poggio, 1986). In general, Gaussian smoothing is the convolution of a Gaussian window and a 1-D vector of data. The Gaussian smoothing $F(x)$ of a signal, $f(x)$, is defined as:

Journal of Structural Engineering. Submitted May 4, 2012; accepted November 28, 2012;
posted ahead of print December 1, 2012. doi:10.1061/(ASCE)ST.1943-541X.0000781

$$F(x) = f(x) * g(x,\sigma) = \int_{-\infty}^{\infty} f(\mu)\, g(x-\mu,\sigma)\, d\mu = \int_{-\infty}^{\infty} f(\mu) \frac{1}{\sqrt{2\pi}\sigma} \exp\left[-\frac{(x-\mu)^2}{2\sigma^2}\right] d\mu \quad (2)$$

where "*" denotes convolution with respect to x, $g(x,\sigma)$ is the Gaussian function with the standard deviation σ, and μ is a dummy variable. These filtering parameters, in addition to window span, should be properly selected to clarify the trend of the *b*-value.

CRACK CLASSIFICATION

In the last two decades, several efforts have been made to correlate AE features with the cracking mode in RC members, which adversely affects structural performance in various ways such as durability and serviceability. In order to utilize the performance-based concept in design more efficiently, the clarification of cracking is quite important. In general, in loading such structures until failure, tensile cracks develop at the initial stages of loading, while shear cracks dominate later (Yuyama et al., 1999). Therefore, it may be beneficial to monitor the mode of the cracks, as it can lead to a prediction of the structural performance. The Japan Construction and Material Standard (JCMS-III B5706, 2003) proposed a technique to monitor the crack propagation in concrete structures based on two AE parameters, namely: "Average Frequency (AF)" and the "RA" value, which are defined as (see Figure 1):

RA = (Rise time) / (Peak Amplitude) (3)

AF = (Counts) / Duration (4)

By using these two parameters, classification of cracks into tensile and other-type signals including shear cracks is performed as illustrated in Figure 2 (Ohtsu 2010). Classification based on these features produce results less dependent on the type of sensors (Ohtsu 2010, Soulioti et

Journal of Structural Engineering. Submitted May 4, 2012; accepted November 28, 2012;
posted ahead of print December 1, 2012. doi:10.1061/(ASCE)ST.1943-541X.0000781

al., 2009, Ohtsu and Tomoda 2008, Ohno and Ohtsu, 2010). However, a defined criterion on the proportion of the RA value and average frequency for crack classification has not yet been confirmed (Ohno and Ohtsu, 2010). In this research, a different approach based on a *k*-means algorithm is proposed to automatically classify the AE signals in two dominant clusters, namely shear and tensile.

k-means Analysis

The *k*-means is one of the simplest unsupervised pattern recognition algorithms that can be used to solve the well-known clustering problem. The *k*-means aims at partitioning datasets into *k* disjoint subsets (clusters) based on minimization of a criterion. The most common clustering criterion is the summation of square distance of each data point in a subset to the center of the subset in which it is partitioned (Likas et al., 2003). The algorithm can be briefly described as follows:

Consider a dataset X=$\{x_1, x_2, \ldots, x_N\}$, $x_n \in R^d$. *k*-means aims at partitioning this dataset into *k* disjoint subsets, $C_1, \ldots, C_k$, through minimizing the criterion or clustering error as follows (Likas et al., 2003):

$$E(m_1, m_2, \ldots, m_k) = \sum_{i=1}^{N} \sum_{j=1}^{k} I(x_i \in C_j) \left\| x_i - m_j \right\|^2 \quad (5)$$

where m_j is the center of j^{th} cluster, C_j, and $I(X)$=1 if X is true and 0 otherwise. This criterion can be minimized through an iterative procedure summarized in the following steps:

1. Initializing *k* centers,$\{m_1, \ldots, m_k\}$, through randomly dividing the dataset into *k* groups and calculating the mean value for each subset.

Journal of Structural Engineering. Submitted May 4, 2012; accepted November 28, 2012;
posted ahead of print December 1, 2012. doi:10.1061/(ASCE)ST.1943-541X.0000781

2. Assigning each data point, x_n, to a cluster, C_j, that its center, m_j, has the lowest Euclidean distance to the point among other cluster centers.
3. Re-computing the centers for k clusters, $\{m_1, ..., m_k\}$.
4. If the change in the centers in the two preceding steps is less than a certain threshold, then the algorithm is converged and the iteration is terminated; otherwise return to step 2.

Although this method is a fast iterative algorithm, its main disadvantage is its sensitivity to the initial guess of the cluster's centers. To overcome this issue, the algorithm was repeated 10 times with randomly selected different initial guesses and the results with the least error criterion per Eq. (5) were accepted.

SIFTED *b*-VALUE (S*b*) ANALYSIS

In order to monitor damage condition for each crack mode, a new algorithm called "Sifted *b*-value (S*b*) analysis". The proposed algorithm, which correlate b-value analysis and cluster analysis can provide more information about the evolution of cracks and structural integrity of the RCSW. The flow chart in Figure 3 illustrates the S*b*-value analysis algorithm. It basically consists in the following steps: 1) Sieve crack modes by systematic AE clustering (i.e., *k*-means); 2) calculate the *b*-values for each cluster; 3) apply the Gaussian filtering to elaborate micro-to-macro transition stages for each crack mode.

EXPERIMENTAL TEST SET-UP

The test specimen was a large scale rectangular RC shear wall, named SW1, with a height to width ratio of 0.94, designed based on the seismic provisions of ACI 318-08 (2008). The width and thickness of the specimen were 305 cm (120 in) and 20.3 cm (8 in), respectively. The

Journal of Structural Engineering. Submitted May 4, 2012; accepted November 28, 2012;
posted ahead of print December 1, 2012. doi:10.1061/(ASCE)ST.1943-541X.0000781

horizontal and vertical reinforcement ratio is an intermediate reinforcement ratio of 0.67%. Compressive strength of concrete on the day of the test was 24.8 MPa and the yield and ultimate strength of the reinforcing bars were 464 MPa and 708 MP, respectively (Rocks, 2012). The main components of the AE system included an eight-channel high-speed data acquisition board (MISTRAS Physical Acoustics Corporation Micro-II) and dedicated software for signal processing and storage (AEwin). The test specimen was instrumented with eight AE sensors (i.e., PAC R15α) attached to one face of the wall using hot glue. Sensors were calibrated according to the ASTM E1106-07. Pencil lead break tests were carried out at different distances away from each sensor to see if the sensors are appropriately mounted and receive waveforms (ASTM E2075). Preamplifiers were set at 40 dB gain, analog bandpass filters were adjusted in the interval of 20 kHz to 400 kHz, and a trigger level was set to be 6 *dB* above the noise level of the system. The experimental setup as well as the sensor layout and load protocol is shown in Figure 4. The lateral load was applied to the specimen by two horizontally inclined high force capacity actuators. The specimen was subjected to a displacement controlled reversed cyclic loading with the loading rate of 0.6 mm/sec that conforms to routine practice for earthquake testing of structural components. The loads are applied slowly because strain rate effects are generally not important for component response to earthquake shaking. Nearly all non-blast tests are performed on structural components at very low speeds of loading. The loading protocol consisted of twelve load steps (LS). In particular, the first load step (LS0) had three cycles whereas the subsequent load steps had two cycles, as shown in Figure 4c. LS0 was carried out to verify the functionality of the experimental setup; because very low AE activity was recorded during this load step, data in LS0 were neglected in the post-processing analyses. In addition, because the last load step (LS11) was a monotonic pull to failure, AE data recorded during this

Journal of Structural Engineering. Submitted May 4, 2012; accepted November 28, 2012;
posted ahead of print December 1, 2012. doi:10.1061/(ASCE)ST.1943-541X.0000781

step were also not considered within the AE analysis in cyclic loading. After reaching the peak load in every cycle, the actuators' load was kept constant for approximately twenty minutes to allow for the cracks to be mapped and photographs to be taken.

EXPERIMENTAL RESULTS

Structural Response and Damage States

The force-displacement hysteresis loops from LS1 to LS10 and the corresponding backbone curves are illustrated in Figure 5. As can be observed, the specimen exhibited a nonlinear response in LS7 and reached its maximum capacity in LS9. Cracking patterns at the peak load of each first cycle, from LS1 to LS10, are shown in Figure 6. The cracking patterns at the negative load peaks were consistent with the photographs due to the symmetric behavior of the wall; therefore they are not reported for the sake of clarity. Flexural (tensile) and shear cracks are indicated with blue and black lines, respectively. In addition, maximum and modal (i.e., appearing most frequently) crack widths are marked in each photograph with a square dot (□) and with a circle (○), respectively. It can be observed that the maximum crack width always occurred in the bottom corners of the specimen, whereas the modal cracks occurred in the diagonal cracks. The maximum and modal cracks widths are plotted in Figure 7 for each load step. Micro-to-macro cracks transition stages are separated by dashed vertical line. The maximum crack width was less than 1 mm between LS1 and LS6. It can be observed that though numerous cracks were formed in the specimen during these loading steps (see Figure 6), the widths of the cracks did not significantly change. Only a few number of hairline cracks could be mapped prior to load step 3. Therefore, it could be inferred that micro-cracks were nucleating in those load steps. From load steps 3 to 6, a lot of visible cracks were observed. It means micro-

Journal of Structural Engineering. Submitted May 4, 2012; accepted November 28, 2012;
posted ahead of print December 1, 2012. doi:10.1061/(ASCE)ST.1943-541X.0000781

cracks coalesced and formed macro-cracks. This stage is called macro-cracks formation. Thereafter, the maximum crack width recorded in the subsequent load steps increased up to 3 mm in LS7 and about 4 mm in LS9, as the specimen reached its maximum capacity. This stage is called macro-cracks opening. The results of this Figure 6 will be used to interpret the *b*-value trends.

Table 1 summarizes damage states (DS) observed during the test. Damage states define threshold levels of damage sustained by structural components under earthquake-type loading. Generally, the DS are characterized by direct indicators of damage such as maximum concrete crack width, extent of concrete spalling and crushing, residual displacement due to sliding shear, and reinforcement buckling and fracture (Degala, 2008; Gonzalez de La Rosa et al., 2007; Gulec et al., 2010; Rocks, 2012; Soulioti et al., 2009).

_b_-value Analysis Results

To monitor the fracture process of the specimen during the test, a *b*-value analysis was carried out as explained in section of "*b*-value analysis". In particular, the *b*-value was calculated using groups of n=70 AE signals. Figure 8 shows the *b*-values obtained considering the AE signals recorded by sensor #2 (S2). The estimated probability density function is also indicated. Interestingly, this function fits a Gaussian probability density function fairly well, with mean and standard deviation calculated from the *b*-values data. As can be seen, it is very difficult to identify a trend in the *b*-value results; this difficulty most likely occurred because of the large amount of AE activity (mostly scattering effects) generated by the specimen under the cyclic loadings. Similar results were obtained by other sensors and due to space limitations, are not reported here. Considering that real-time monitoring of large structures requires the capability to

Journal of Structural Engineering. Submitted May 4, 2012; accepted November 28, 2012;
posted ahead of print December 1, 2012. doi:10.1061/(ASCE)ST.1943-541X.0000781

elaborate large amounts of data generated from the structure during normal operating conditions, in this research it is proposed to filter the *b*-value data using a Gaussian moving average as described in the section of "Gaussian Filters".1. In particular, the window span was defined as about 5% of the length of the data vector (e.g., 225 for S2 that has almost 4,500 data) while the standard deviation was set to about a quarter of the window span. Figure 9 shows the outcome of the filtering process applied to all data recorded by each sensor during the test (i.e., S1-S8); the corresponding load steps are also indicated. As mentioned before, in general, the *b*-value increases during the formation of micro-cracks (i.e., early stages of damage) and decreases when the macro-cracks begin to localize (Colombo et al., 2003). In Figure 9, a decreasing trend indicating that macro-cracks are localizing (i.e., damage accumulation) can be observed in some sensors (i.e., S1, S2, S3, S4, S6), which is shown with an arrow. A dashed line indicates the beginning of the decreasing trend. Note that this trend appears more evident for sensors 1, 2 and 3 located in proximity to the bottom corners of the specimen, where the maximum crack widths were measured (see Figure 6); furthermore, it starts in LS6 or LS7, where the transition of the mechanical behavior of the specimen from linear to nonlinear occurred (see Figure 5). Sensors 4 and 6 were mounted at 0.8 m above the first row of sensors and close to the edges of the wall where the initial flexural cracks were followed by diagonal shear cracks. A decreasing trend can be observed in sensor 4 in LS8; this could have been caused by the nucleation of a new crack in proximity to this sensor in LS8 (see Figure 6) and by the opening of other cracks that increased the severity of damage in that area. A sudden drop occurred in S6 at LS9 where the wall reached its maximum capacity. Interestingly, for S4 and S6, the *b*-value began to decrease later than in S1, S2 and S3; therefore it is reasonable to assume that damage is progressing from the bottom of the specimen upward. The other sensors (S5, S7, and S8) do not show a clear trend in

Journal of Structural Engineering. Submitted May 4, 2012; accepted November 28, 2012;
posted ahead of print December 1, 2012. doi:10.1061/(ASCE)ST.1943-541X.0000781

comparison to other channels. Thus, it can be concluded that most of the damage was localized in the bottom part of the specimen.

Figure 10 shows the *b*-value results obtained considering the entire dataset (i.e., *b*-values obtained using data collected by all sensors) without the filtering process, along with the corresponding probability density function. Figure 11 shows the outcome of the filtering process with the damage states indicated. The *b*-value direction is highlighted by a dashed line.

It is interesting to compare the *b*-value trend with the damage states (Table 1) and progression of crack widths (Figure 7). It can be inferred that as long as the maximum measured crack width was less than 0.5 mm (DS1) and micro-cracks were nucleating up to LS3, the trend generally increased, whereas formation of macro-cracks and yielding in web and boundary element reinforcement (DS2) led to a generally plateau trend with periodically oscillation around a mean value of 1.32 between LS3 and LS5. Considering that the load protocol consisted of loading and unloading cycles, it is reasonable to assume this oscillation is caused by AE activities generated by secondary AE sources including friction at the interface of the cracks and rebar-concrete during the unloading phases (i.e., *b*-value ascends), and formation of macro-cracks (i.e., *b*-value descends) during the loading phases. The opening of macro-cracks and concrete crushing mostly occurred from LS7 (DS3) onward and the corresponding *b*-values follow a generally descending trend. Interestingly, the minimum *b*-value was obtained in DS4 as the specimen reached its ultimate strength and slid against its base; that is, in LS9 (see Figure 5 and Table 1). An unstable *b*-value was observed in LS10; at this stage, the specimen was severely damaged and widths of shear cracks exceeded 3 mm. As a result, a decreasing trend of the *b*-value may be used as an indication of damage accumulation within the structure. The maximum, minimum, and

Journal of Structural Engineering. Submitted May 4, 2012; accepted November 28, 2012;
posted ahead of print December 1, 2012. doi:10.1061/(ASCE)ST.1943-541X.0000781

percentage drop of *b*-value for the sensors that show a significant decrease and all sensors together are reported in Table 2. Average and median of this percentage drop conclude the critical value of 81% as the sign of serious damage and indicator of macro-crack development.

Crack Classification Results

In this section, the results of the crack classification using the *k*-means analysis are presented. For each load step, the two features defined in Eq. (3) and Eq. (4) (i.e., RA and AF) were extracted from each AE signal. A moving average with a window span and lag of 70 AE signals was carried out on these two features before the *k*-means analysis.

As a result, a dataset **X** consisting of data points $x_i = (\overline{RA}_i, \overline{AF}_i)$ was generated; that is, $X = \{(\overline{RA_1}, \overline{AF_1}), (\overline{RA_2}, \overline{AF_2}), \ldots, (\overline{RA_n}, \overline{AF_n})\}$, $x_i \in R^2$. Typical variation ranges of the RA value and average frequency (AF) found in the literature for concrete elements are AF=60 kHz and RA=2000 μs/V for 150 kHz resonant sensors (Soulioti et al., 2009; Gonzalez de La Rosa et al., 2007; Degala, 2008). In this research, the average frequency of the signals was about 40 kHz and the average of the RA values was in the range of 5-15 μsec/dB during the nonlinear load steps using R15 resonance transducers.

It is worthy noting that *k*-means, as other types of clustering analysis, does not guarantee that each point in the same cluster is effectively generated by the corresponding crack mode. The proposed cluster analysis provides an estimate of which type of AE events are dominant, shear or tensile. For instance, friction type signals that mostly occur during unloading have characteristics similar to shear type signals and thus they will be inevitably included in the shear cluster. However it does not impair damage state estimation based on clustering because with the

Journal of Structural Engineering. Submitted May 4, 2012; accepted November 28, 2012;
posted ahead of print December 1, 2012. doi:10.1061/(ASCE)ST.1943-541X.0000781

evolution of damage AE activity during unloading (friction-type signals) becomes more intense. Therefore, accumulation of shear cracks and friction type signals that result in domination of shear class can be considered as indicator of damage progression (Shah and Ribakov, 2010, Ohtsu et al., 2002,Colombo et al., 2005, Aggelis et al., 2010).

The proposed clustering analysis was applied to partition the dataset X into two subsets (i.e., k=2), named cluster 1 (i.e., tensile cracks) and cluster 2 (i.e., shear cracks). For the sake of clarity, the results of the k-means analysis are presented only for the dataset recorded in LS4 and LS5, (Figure 12). From Figure 12a, it can be observed that in LS4, the total number of elements in the first cluster (i.e., tensile cracks) is larger than the number of elements in the second one (i.e., shear cracks); an opposite trend can be observed in Figure 12b. Therefore, it is reasonable to assume that tensile cracks were dominant in LS4, whereas shear cracks were dominant in LS5. It can be seen that this method is capable of systematically classifying the dataset into two clusters without the need to manually assign a line for partitioning. Since the summation of the square distance to each center is the criterion to be minimized, the relative order of magnitude of the two features plays an important role. In this research, it is proposed to consider the dimensions of RA and AF as [μsec/dB] and [kHz], respectively. In Figure 13, the total number of elements in each cluster is shown for each load step. It can be observed that tensile cracks were dominant up to LS4, whereas shear cracks became dominant from LS5 to failure. A similar conclusion may be obtained by inspection of crack patterns observed in each load step (see Figure 6).

S*b*-Value Results

In order to track the micro-to-macro crack transition stages for each crack mode, Figure 14

Journal of Structural Engineering. Submitted May 4, 2012; accepted November 28, 2012;
posted ahead of print December 1, 2012. doi:10.1061/(ASCE)ST.1943-541X.0000781

shows the results of the S*b*-value analysis for both classes. The following observations can be made: 1) an initial increasing trend indicates formation of tensile micro-cracks until LS3 (figure 14a) and shear micro-cracks until LS5 (figure 14b); 2) macro-cracks opening begins in LS5 for tensile cracks and in LS7 for shear cracks; interestingly in LS7 onset of nonlinearity occurred (see Figure 5). Therefore a general delay in damage progression is observed between these modes. In another word, transition conditions for tensile cracks occur earlier than shear cracks, that is, tensile cracks are followed by shear cracks. As a result, onset of decreasing trend in tensile S*b*-values (LS 5 in Figure 14a) could be considered as an early warning for proximity to yielding at LS7. Furthermore, both fracture modes reached their minimum *b*-value at LS9 where the wall disclosed its ultimate lateral strength.

CONCLUSION

Reinforced Concrete (RC) shear walls are popular gravity and lateral force resisting systems. Failure of a shear wall may result in severe damage and even progressive collapse of a concrete structure. In this paper, an experimental study to monitor the fracture process in a RC shear wall subjected to cyclic loading has been described. The proposed system is based on a sparse array of Acoustic Emission (AE) sensors to continuously monitor the structure under investigation. In particular, a *b*-value analysis has been presented to monitor the propagation of cracks during the test. A Gaussian filter has been proposed to improve the interpretation of the *b*-value data. In addition, a cluster analysis based on the *k*-means is presented to automatically classify the two fundamental crack modes (i.e., tensile and shear). A novel algorithm called Sifted b-value analysis is introduced to provide detailed information about the evolution of each crack mode. The following observations and conclusions have been obtained:

Journal of Structural Engineering. Submitted May 4, 2012; accepted November 28, 2012;
posted ahead of print December 1, 2012. doi:10.1061/(ASCE)ST.1943-541X.0000781

- A Gaussian moving average has been successfully proposed to improve the interpretation of the *b*-value results.
- The *b*-value analysis was capable of identifying the damage progression in the specimen. The minimum *b*-value was observed when the specimen reached its maximum strength capacity.
- The cluster analysis based on the *k*-means was successfully applied to automatically classify the AE sources as tensile or shear cracks.
- Sifted b-value analysis could monitor the evolution of each crack mode and provide early warning for onset of yielding.

ACKNOWLEDGMENTS

The authors acknowledge the National Science Foundation (NSF) for providing the financial support for this project under Grant No. CMMI-0829978. The experiments presented herein could not have been completed without contributions from the staff of the Structural Engineering and Earthquake Simulation Laboratory (SEESL) of the University at Buffalo, State University of New York. The authors also acknowledge the advice and help provided by the technical staff at the NEES Equipment Site at the University at Buffalo, State University of New York.

REFERENCES

ACI Committee 318. (2008). Building Code Requirements for Structural Concrete (ACI 318-08) and Commentary, American Concrete Institute, ISBN: 978-0-87031-264-9

Aggelis, D. G. (2011). "Classification of cracking mode in concrete by acoustic emission parameters." *Mechanics Research Communications*, 38(3), 153-157.

Journal of Structural Engineering. Submitted May 4, 2012; accepted November 28, 2012;
posted ahead of print December 1, 2012. doi:10.1061/(ASCE)ST.1943-541X.0000781

Aggelis, D. G., Shiotani, T., and Terazawa, M. (2010). "Assessment of Construction Joint Effect in Full-Scale Concrete Beams by Acoustic Emission Activity." Journal of Engineering Mechanics, 136(7), 906–912.

ASTM E1106 – 07, Standard Test Method for Primary Calibration of Acoustic Emission Sensors, *American Society for Testing and Materials* (*ASTM*), DOI: 10.1520/E1106-07.

ASTM E2075 / E2075M – 10, Standard Practice for Verifying the Consistency of AE-Sensor Response Using an Acrylic Rod, *American Society for Testing and Materials*, DOI: 10.1520/E2075_E2075M-10

Carpinteri, A., Lacidogna, G., Niccolini, G., and Puzzi, S. (2007). "Critical defect size distributions in concrete structures detected by the acoustic emission technique." *Meccanica*, 43(3), 349-363.

Colombo, I. S., Main, I. G., and Forde, M. C. (2003). "Assessing Damage of Reinforced Concrete Beam Using " *b* -value " Analysis of Acoustic Emission Signals." *ASCE Journal of Materials in Civil Engineering*, 15(3), 280-286.

Colombo, S. Forde, M. C., Main, I. G., Halliday, J., Shigeishi, M. (2005). "AE energy analysis on concrete bridge beams." Materials and Structures, 38(283), 851–856.

Degala, S. (2008). "Acoustic Emission Monitoring of Reinforced Concrete Systems Retrofitted with CFRP." M.Sc. Thesis, Swanson School of Engineering, University of Pittsburgh, Pennsylvania, USA.

Journal of Structural Engineering. Submitted May 4, 2012; accepted November 28, 2012;
posted ahead of print December 1, 2012. doi:10.1061/(ASCE)ST.1943-541X.0000781

Farhidzadeh, A., Salamone, S., Luna, B., and Whittaker, A. (2012). "Acoustic Emission Monitoring of a Reinforced Concrete Shear Wall by *b*- value based Outlier Analysis." *Structural Health Monitoring*, In press, doi: 10.1177/1475921712461162.

Godin, N. (2004). "Clustering of acoustic emission signals collected during tensile tests on unidirectional glass/polyester composite using supervised and unsupervised classifiers." *NDT & E International*, 37(4), 253-264.

Godin, N., Huguet, S., and Gaertner, R. (2005). "Integration of the Kohonen's self-organising map and -means algorithm for the segmentation of the AE data collected during tensile tests on cross-ply composites." *NDT & E International*, 38(4), 299-309.

Gonzalez de La Rosa, J., Piotrkowski, R., and Ruzzante, J. (2007). "Third-order spectral characterization of acoustic emission signals in ring-type samples from steel pipes for the oil industry." *Mechanical Systems and Signal Processing*, 21(4), 1917-1926.

Grosse, C. U., and Ohtsu, M. (2008). Acoustic Emission Testing – Basics for Research Applications in Civil Engineering, Springer Verlag, Berlin & Heidelberg, Germany

Gulec, C. K., Whittaker, A. S., and Hooper, J. D. (2010). "Fragility functions for low aspect ratio reinforced concrete walls." *Engineering Structures*, Elsevier Ltd, 32(9), 2894-2901.

Gutenberg, B., and Richter, C. F. (1949). Seismicity of the earth and associated phenomena, in Frequency and Energy of Earthquakes. Princeton, NJ, Princeton University Press, 17-19.

Journal of Structural Engineering. Submitted May 4, 2012; accepted November 28, 2012;
posted ahead of print December 1, 2012. doi:10.1061/(ASCE)ST.1943-541X.0000781

Hardy, H. R. J. (1972). "Application of acoustic emission techniques to rock mechanics research." *ASTM STP 505*, ASTM Publ., 41-83.

Holford, K. M., and Lark, R. J. (2005). "Acoustic Emission testing of bridges, in Inspection and monitoring techniques for bridges and structures." G. Fu, ed., Woodhead Publishing Ltd., Cambridge, UK.

JCMS-IIIB5706. (2003). "Japan Construction Material Standards." Monitoring Method for Active Cracks in Concrete by Acoustic Emission. The Federation of Construction Material Industries, Japan.

Kostopoulos, V. (2003). "On the identification of the failure mechanisms in oxide/oxide composites using acoustic emission." *NDT & E International*, 36(8), 571-580.

Kurz, J. H. (2006). "Stress Drop and Stress Redistribution in Concrete Quantified Over Time by the b-value Analysis." *Structural Health Monitoring*, 5(1), 69-81.

Likas, A., Vlassis, N., and J. Verbeek, J. (2003). "The global k-means clustering algorithm." *Pattern Recognition*, 36(2), 451-461.

Lin, H.C., Wang, L.L., and Yang, S.N. (1996). "Automatic determination of the spread parameter in Gaussian smoothing." *Pattern Recognition Letters*, 17(12), 1247-1252.

Manson, G., Worden, K., Holford, K., and Pullin, R. (2001). "Visualisation and Dimension Reduction of Acoustic Emission Data for Damage Detection." *Journal of Intelligent Materials Systems and Structures*, 12(8), 529-536.

Journal of Structural Engineering. Submitted May 4, 2012; accepted November 28, 2012;
posted ahead of print December 1, 2012. doi:10.1061/(ASCE)ST.1943-541X.0000781

Miller, R. K., and Hill, E. (2005). Acoustic emission testing. Nondestructive testing handbook, 3rd edition: vol. 6, P. O. Moore, ed., ASNT, Columbus, OH, 1-25.

Ohno, K., and Ohtsu, M. (2010). "Crack classification in concrete based on acoustic emission." *Construction and Building Materials*, Elsevier Ltd, 24(12), 2339-2346.

Ohtsu, M. (2010). "Recommendation of RILEM TC 212-ACD: acoustic emission and related NDE techniques for crack detection and damage evaluation in concrete." RILEM Technical Committee, 43(9), 1187–1189.

Ohtsu, M., & Tomoda, Y. (2008). "Phenomenological Model of Corrosion Process in Reinforced Concrete Identified by Acoustic Emission". ACI Materials Journal, 105(2), 194-199

Ohtsu, M., Uchida, M., Okamoto, T., & Yuyama, S. (2002). "Damage Assessment of Reinforced Concrete Beams Qualified by Acoustic Emission". ACI Structural Journal, (99), 411–417

Pappas, Y. Z., Markopoulos, Y. P., and Kostopoulos, V. (1998). "Failure mechanisms analysis of 2D carbon / carbon using acoustic emission monitoring." *NDT&E International*, 31(3), 157-163.

Paterson, J. (2001). "Seismic Retrofit of Reinforced Concrete Shear walls." McGill University, Montreal, Canada.

Priestley, M. J. N., and Seible, F. (1996). "Design of seismic retrofit measures for concrete and masonry structures." Construction and Building Materials, 9(6), 365–377.

Journal of Structural Engineering. Submitted May 4, 2012; accepted November 28, 2012;
posted ahead of print December 1, 2012. doi:10.1061/(ASCE)ST.1943-541X.0000781

Rocks, J. F. (2012). "Large Scale Testing of Low aspect Ratio Reinforced Concrete Walls." M.Sc. Thesis, Department of Civil, Structural and Environmental Engineering, University at Buffalo, NY.

Salamone, S., Veletzos, M. J., Lanza di Scalea, F., and Restrepo, J. I. (2012). "Detection of Initial Yield and Onset of Failure in Bonded Post-Tensioned Concrete Beams." *Journal of Bridge Engineering*, 17(6), 1-9.

Shah, A. A., & Ribakov, Y. (2010). Effectiveness of nonlinear ultrasonic and acoustic emission evaluation of concrete with distributed damages. Materials & Design, 31(8), 3777–3784.

Schumacher, T., Higgins, C. C., and Lovejoy, S. C. (2010). "Estimating Operating Load Conditions on Reinforced Concrete Highway Bridges with b-value Analysis from Acoustic Emission Monitoring." *Structural Health Monitoring*, 10(1), 17-32.

Shiotani, T., Yuyama, S., Li, Z. W., and Ohtsu, M. (2001). "Application of AE improved b-value to quantitative evaluation of fracture process in concrete materials." *Journal of Acoustic Emission*, 19, 118-133.

Soulioti, D., Barkoula, N. M., Paipetis, a., Matikas, T. E., Shiotani, T., and Aggelis, D.G. (2009). "Acoustic emission behavior of steel fibre reinforced concrete under bending." *Construction and Building Materials*, Elsevier Ltd, 23(12), 3532-3536.

Watanabe, T., Nishibata, S., Hashimoto, C., and Ohtsu, M. (2007). "Compressive failure in concrete of recycled aggregate by acoustic emission." *Construction and Building Materials*, 21(3), 470-476.

Journal of Structural Engineering. Submitted May 4, 2012; accepted November 28, 2012;
posted ahead of print December 1, 2012. doi:10.1061/(ASCE)ST.1943-541X.0000781

Witkin, A. P. (1984). "Scale-space filtering: A new approach to multi-scale description." *Acoustics, Speech, and Signal Processing, IEEE International Conference on ICASSP '84*, 9, 150-153.

Yuille, a L., and Poggio, T. a. (1986). "Scaling theorems for zero crossings." *IEEE transactions on pattern analysis and machine intelligence*, 8(1), 15-25.

Yuyama, S., Li, Z., Ito, Y., and Arazoe, M. (1999). "Quantitative analysis of fracture process in RC column foundation by moment tensor analysis of acoustic emission." *Construction and Building Materials*, 13, 87-97.

Zhou, H., and Attard, T. L. (2012). "Rehabilitation and strength sustainability of fatigue damaged concrete–encased steel flexural members using a newly developed polymeric carbon–fiber composite." *Composites Part B: Engineering*, Elsevier Ltd.

Journal of Structural Engineering. Submitted May 4, 2012; accepted November 28, 2012;
posted ahead of print December 1, 2012. doi:10.1061/(ASCE)ST.1943-541X.0000781

List of Figures

Journal of Structural Engineering. Submitted May 4, 2012; accepted November 28, 2012;
posted ahead of print December 1, 2012. doi:10.1061/(ASCE)ST.1943-541X.0000781

List of Tables

Journal of Structural Engineering. Submitted May 4, 2012; accepted November 28, 2012;
posted ahead of print December 1, 2012. doi:10.1061/(ASCE)ST.1943-541X.0000781

Table 1. Damage States (DS) and corresponding Load Steps (LS)

ID	Damage states	LS
DS1	Maximum measured crack width less than 0.02 in. (0.5 mm)	LS1-3
DS2	Yielding in web and boundary element reinforcement	LS4
	Maximum measured crack widths larger than 0.5 mm but less than 3 mm	LS4-6
DS3	Concrete crushing at the compression toes/initiation of crushing in the wall web	LS7
	Flexural cracks with widths exceeding 0.12 in. (3 mm)	LS7
DS4	Sliding at the base of the wall	LS9
	Widespread crushing of concrete	LS10
	Shear cracks with widths exceeding 0.12 in. (3 mm)	LS10

Journal of Structural Engineering. Submitted May 4, 2012; accepted November 28, 2012;
posted ahead of print December 1, 2012. doi:10.1061/(ASCE)ST.1943-541X.0000781

Table 2. Percentage of *b*-value drop as indicator of macro-crack opening.

sensor	minimum	maximum	Drop [%]
1	1.075	1.378	78
2	1.073	1.339	80
3	1.271	1.432	89
4	1.232	1.489	82
6	1.303	1.461	89
8	1.134	1.690	67
All sensors	1.110	1.350	82
		Average	81
		median	82

Journal of Structural Engineering. Submitted May 4, 2012; accepted November 28, 2012;
posted ahead of print December 1, 2012. doi:10.1061/(ASCE)ST.1943-541X.0000781

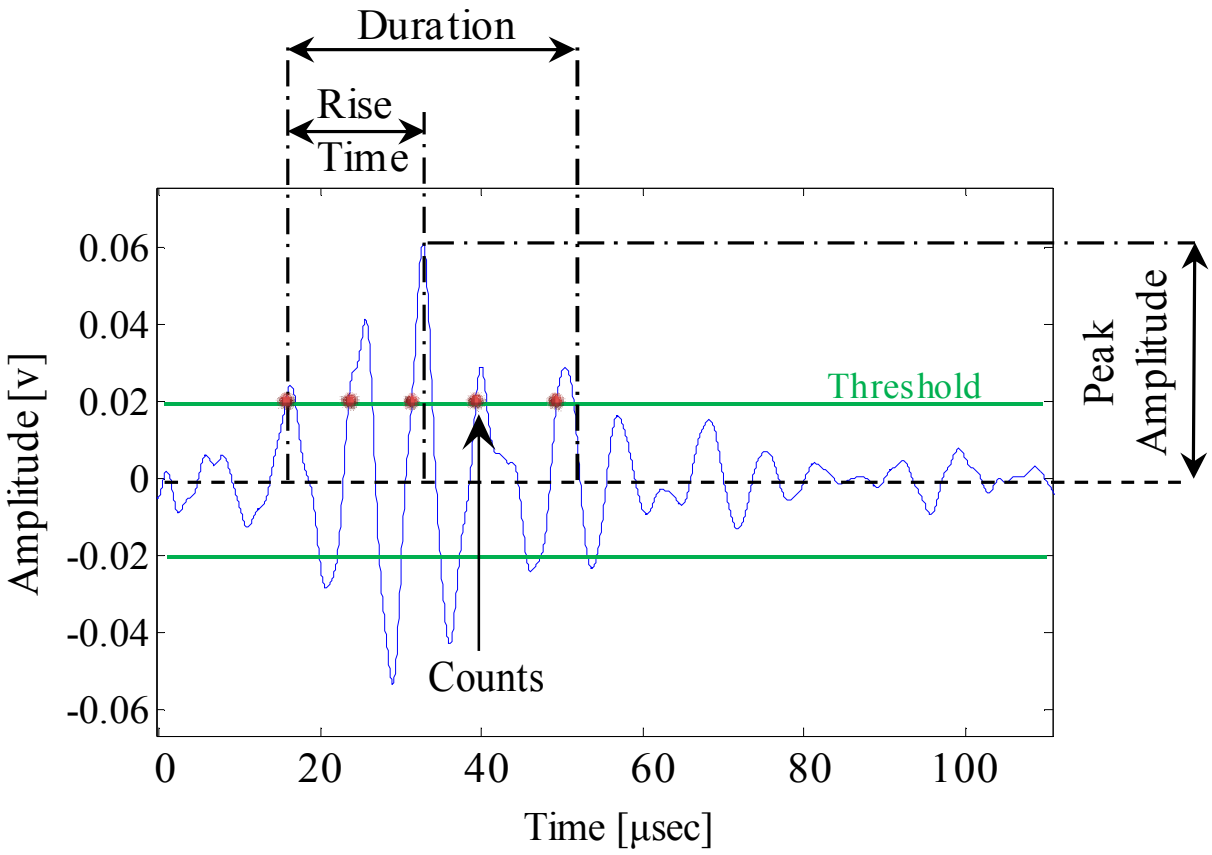

Figure 1. AE signal with features

Journal of Structural Engineering. Submitted May 4, 2012; accepted November 28, 2012;
posted ahead of print December 1, 2012. doi:10.1061/(ASCE)ST.1943-541X.0000781

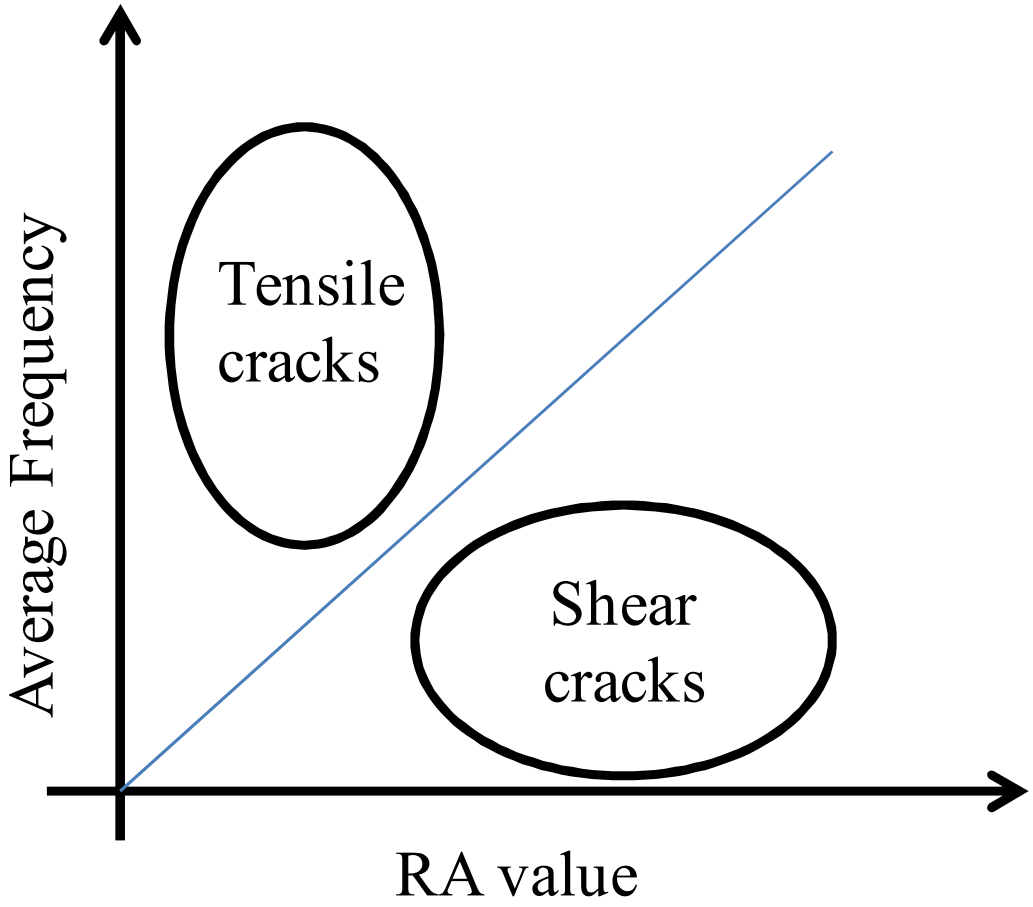

Figure 2. AE Signal Classification (JCMS-IIIB5706 2003)

Journal of Structural Engineering. Submitted May 4, 2012; accepted November 28, 2012;
posted ahead of print December 1, 2012. doi:10.1061/(ASCE)ST.1943-541X.0000781

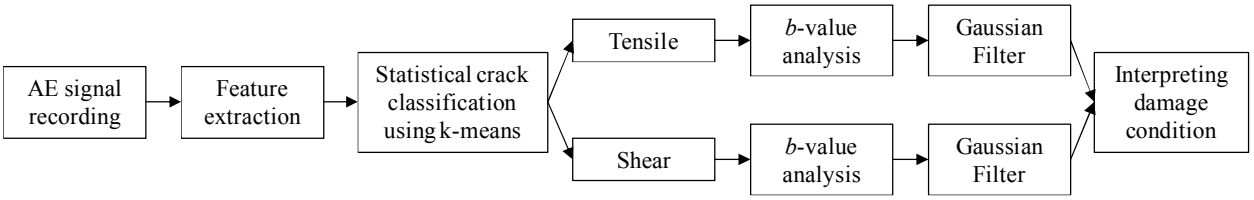

Figure 3. Algorithm of S*b*-value analysis

Journal of Structural Engineering. Submitted May 4, 2012; accepted November 28, 2012;
posted ahead of print December 1, 2012. doi:10.1061/(ASCE)ST.1943-541X.0000781

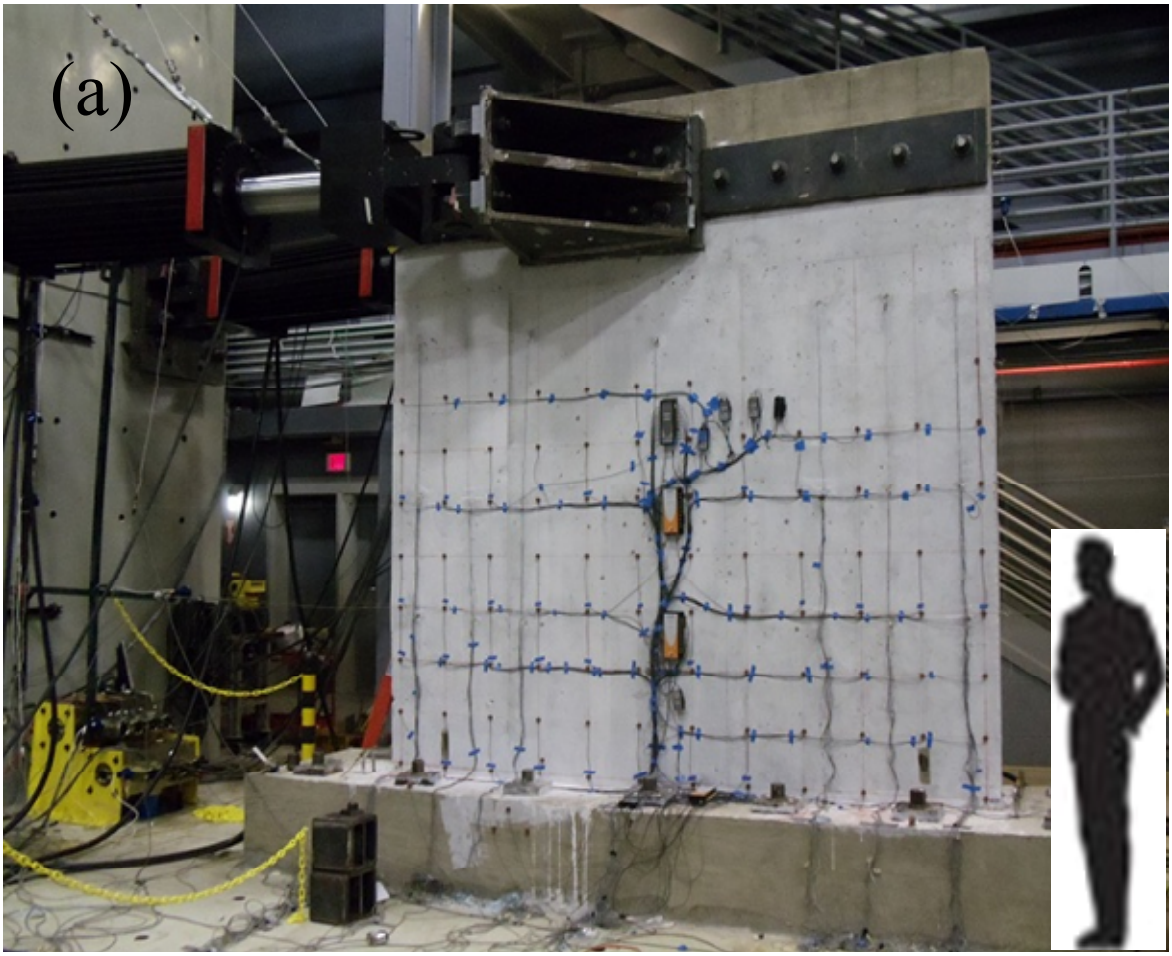

Figure 4. Experimental test: (a) site view and instrumentation; (b) AE sensor layout; (c) load protocol

Journal of Structural Engineering. Submitted May 4, 2012; accepted November 28, 2012;
posted ahead of print December 1, 2012. doi:10.1061/(ASCE)ST.1943-541X.0000781

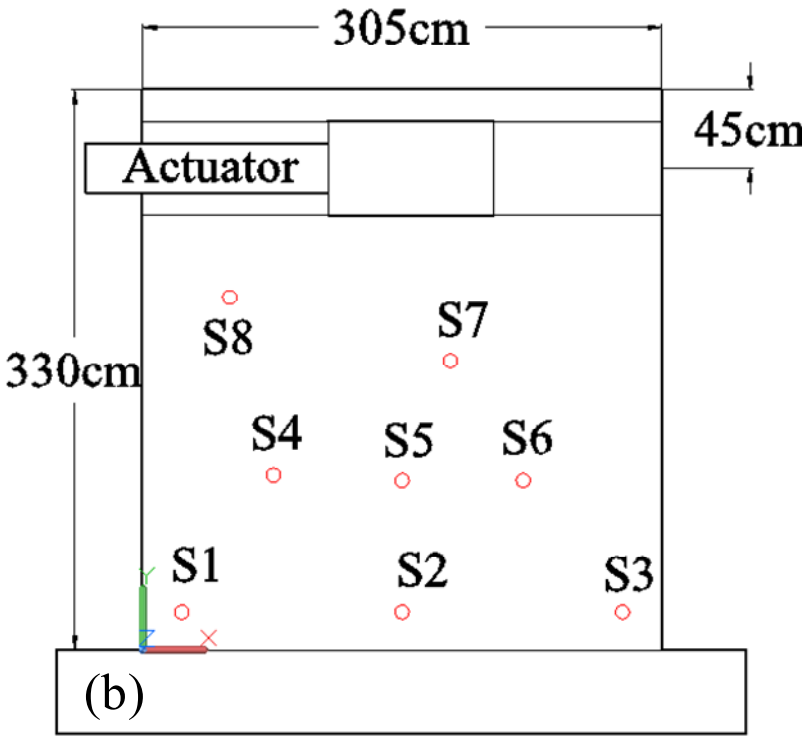

Figure 4. Experimental test: (a) site view and instrumentation; (b) AE sensor layout; (c) load protocol

Journal of Structural Engineering. Submitted May 4, 2012; accepted November 28, 2012;
posted ahead of print December 1, 2012. doi:10.1061/(ASCE)ST.1943-541X.0000781

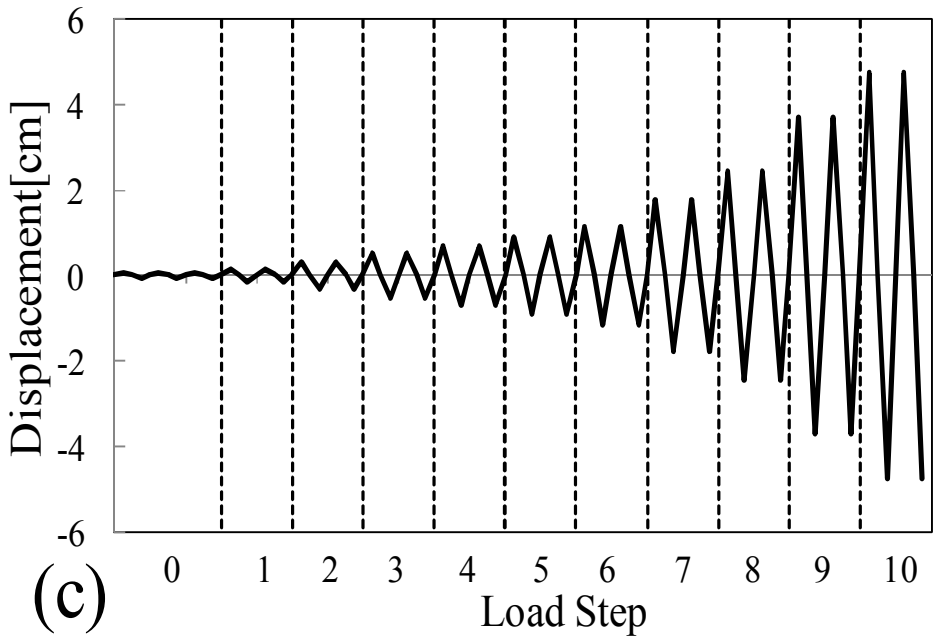

Figure 4. Experimental test: (a) site view and instrumentation; (b) AE sensor layout; (c) load protocol

Journal of Structural Engineering. Submitted May 4, 2012; accepted November 28, 2012;
posted ahead of print December 1, 2012. doi:10.1061/(ASCE)ST.1943-541X.0000781

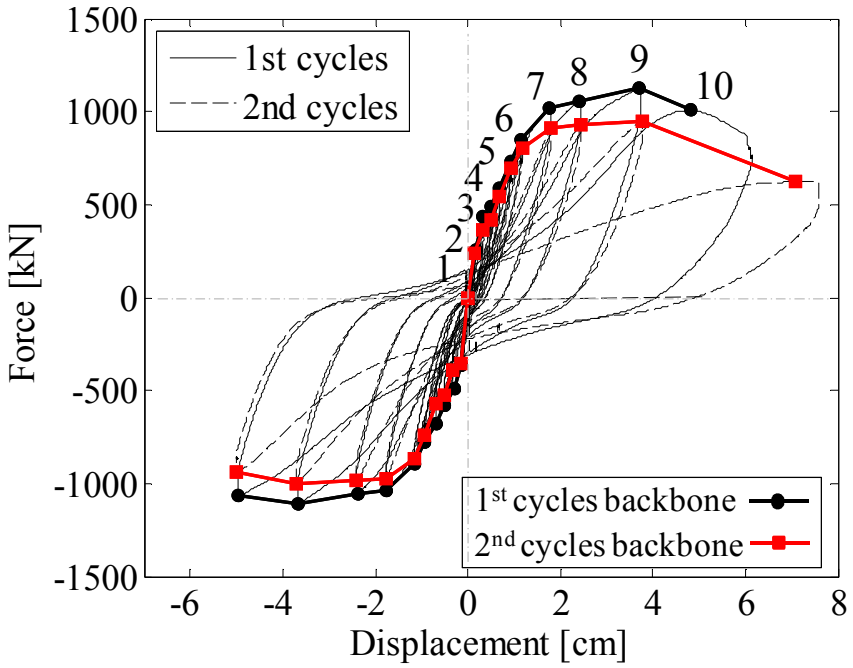

Figure 5. Force-displacement hysteresis loops and backbone curves

Journal of Structural Engineering. Submitted May 4, 2012; accepted November 28, 2012;
posted ahead of print December 1, 2012. doi:10.1061/(ASCE)ST.1943-541X.0000781

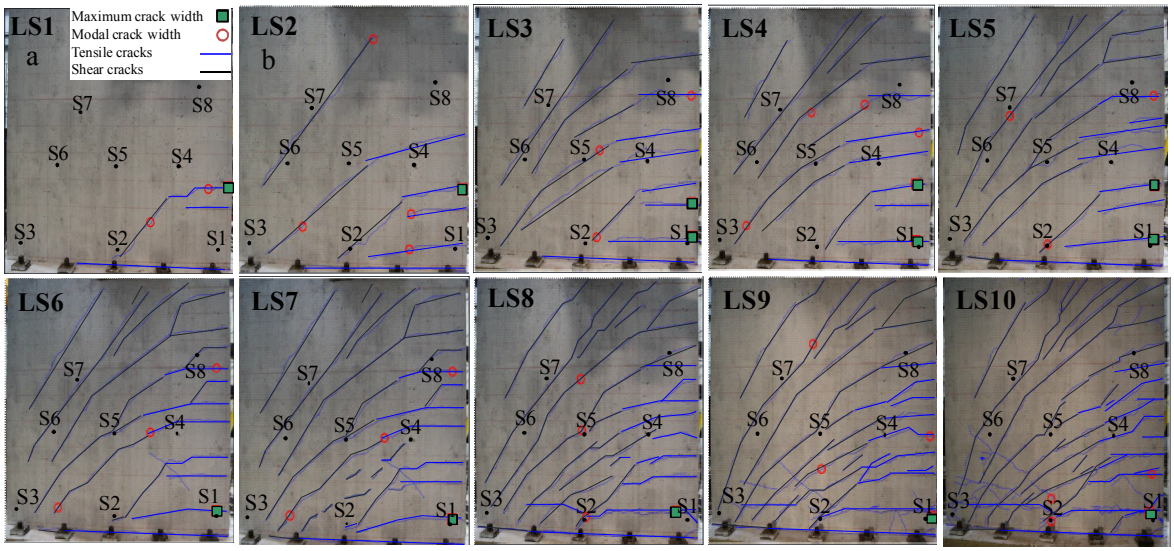

Figure 6. Crack positions, orientation, and mode in the positive peak of 1st cycles from LS1 to LS10

Journal of Structural Engineering. Submitted May 4, 2012; accepted November 28, 2012;
posted ahead of print December 1, 2012. doi:10.1061/(ASCE)ST.1943-541X.0000781

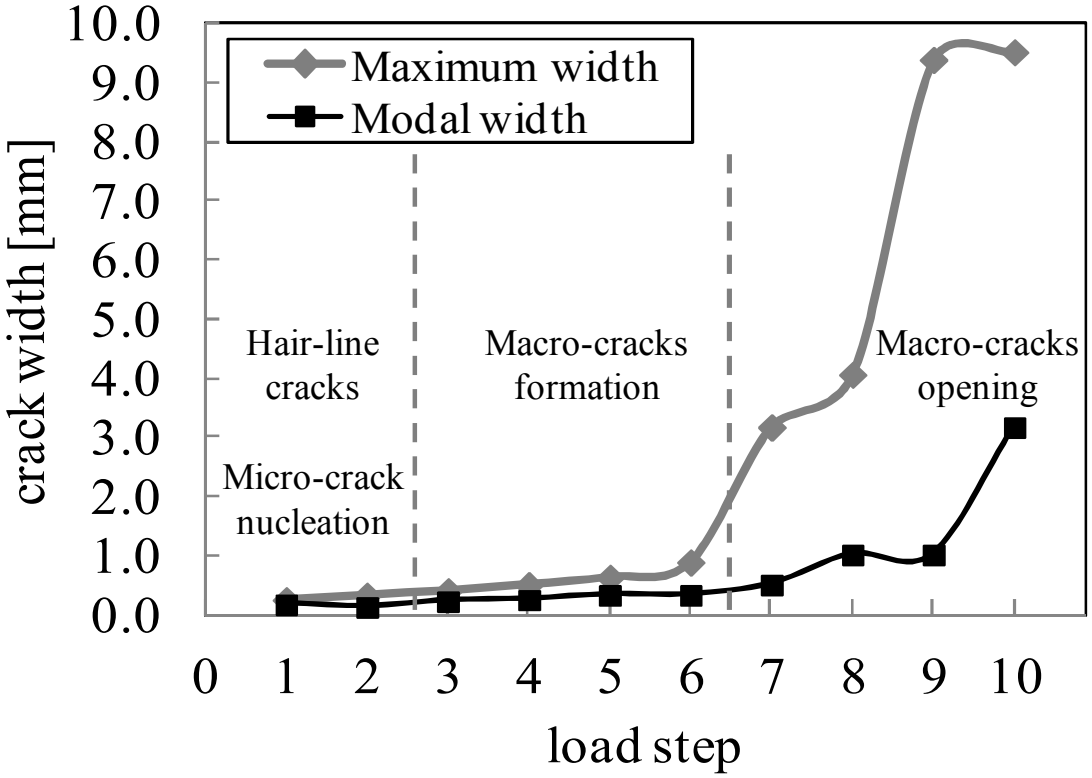

Figure 7. Maximum and modal cracks widths vs. load steps

Journal of Structural Engineering. Submitted May 4, 2012; accepted November 28, 2012;
posted ahead of print December 1, 2012. doi:10.1061/(ASCE)ST.1943-541X.0000781

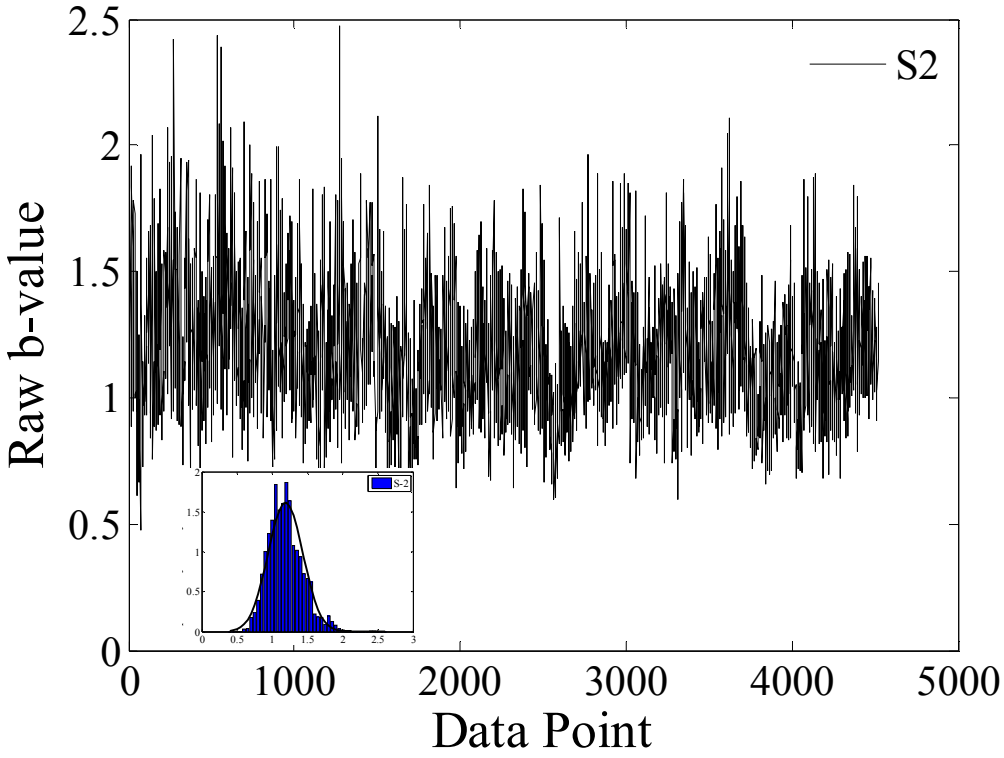

Figure 8. *b*-value results for sensor #2

Journal of Structural Engineering. Submitted May 4, 2012; accepted November 28, 2012;
posted ahead of print December 1, 2012. doi:10.1061/(ASCE)ST.1943-541X.0000781

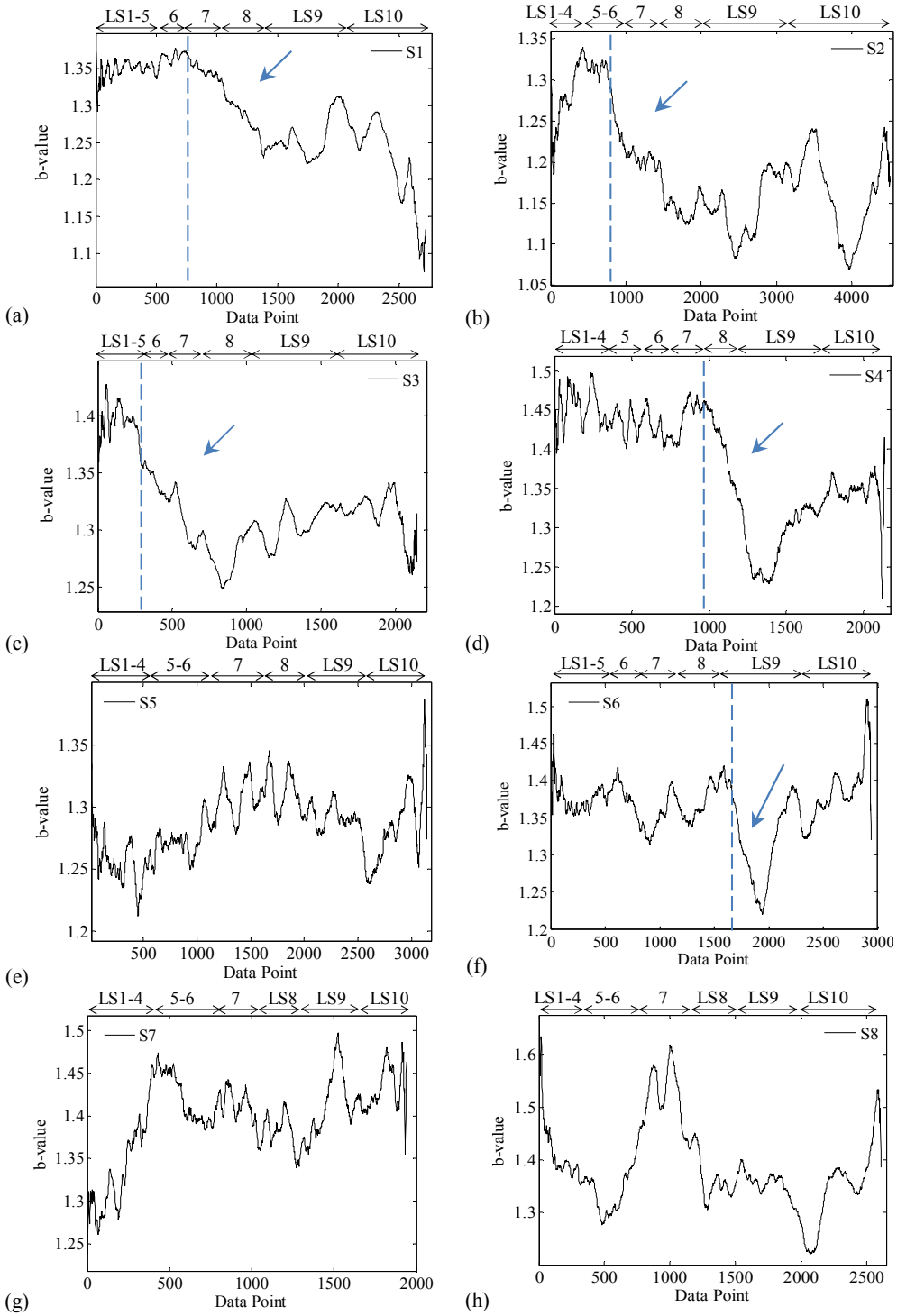

Figure 9. *b*-value results for each sensor after Gaussian filtering

Journal of Structural Engineering. Submitted May 4, 2012; accepted November 28, 2012;
posted ahead of print December 1, 2012. doi:10.1061/(ASCE)ST.1943-541X.0000781

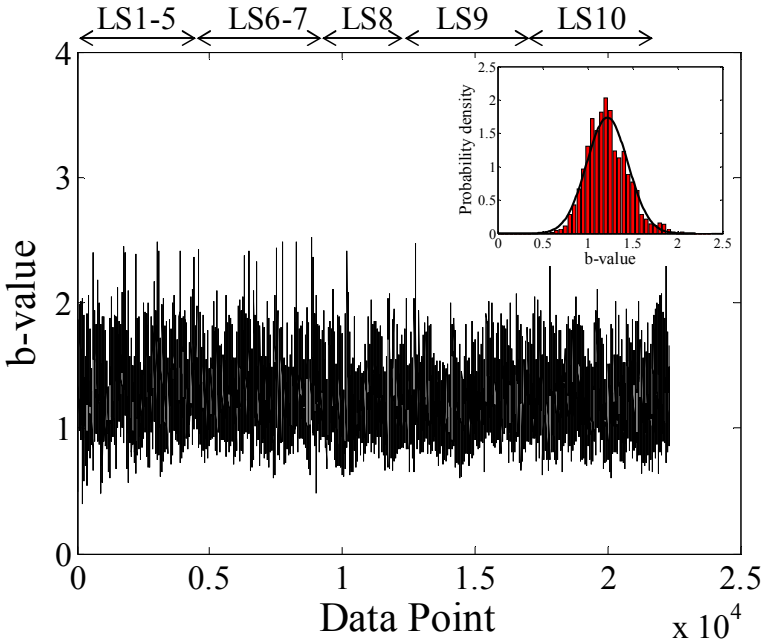

Figure 10. *b*-values results for the entire dataset before filtering process

Journal of Structural Engineering. Submitted May 4, 2012; accepted November 28, 2012;
posted ahead of print December 1, 2012. doi:10.1061/(ASCE)ST.1943-541X.0000781

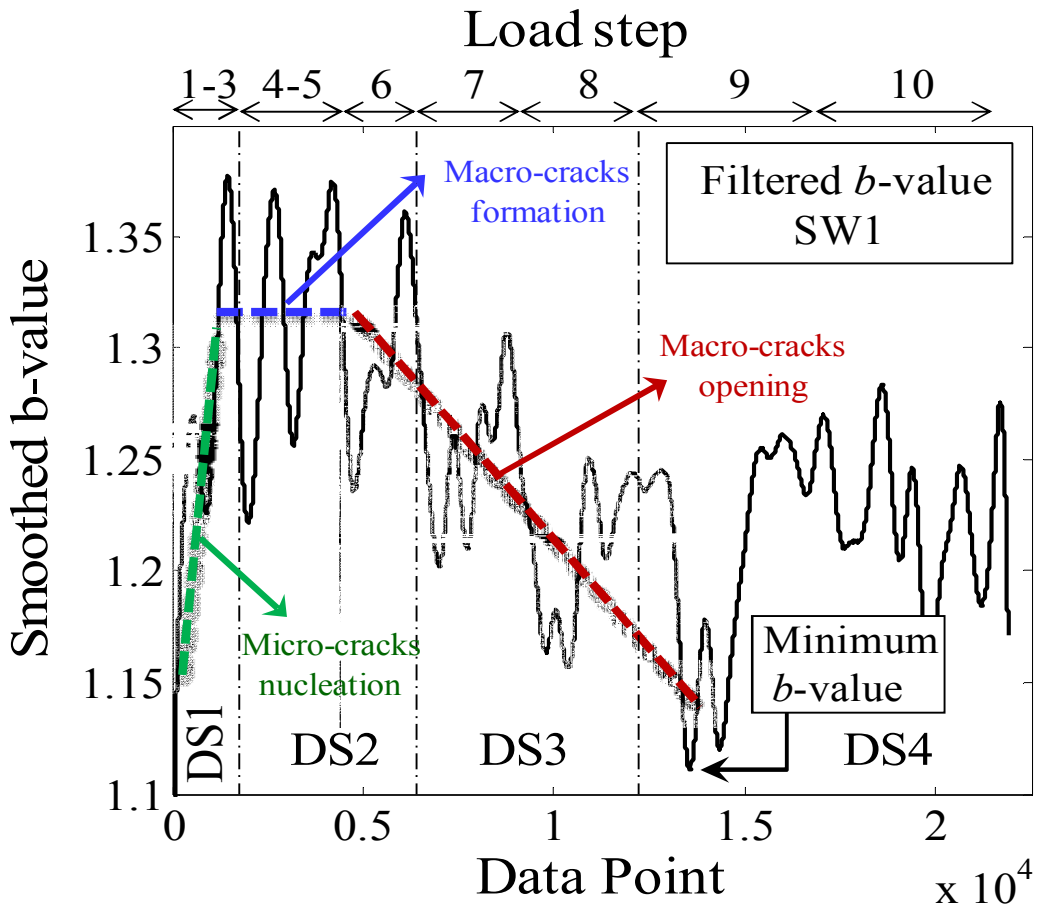

Figure 11. Smoothed *b*-values for the entire dataset

Journal of Structural Engineering. Submitted May 4, 2012; accepted November 28, 2012;
posted ahead of print December 1, 2012. doi:10.1061/(ASCE)ST.1943-541X.0000781

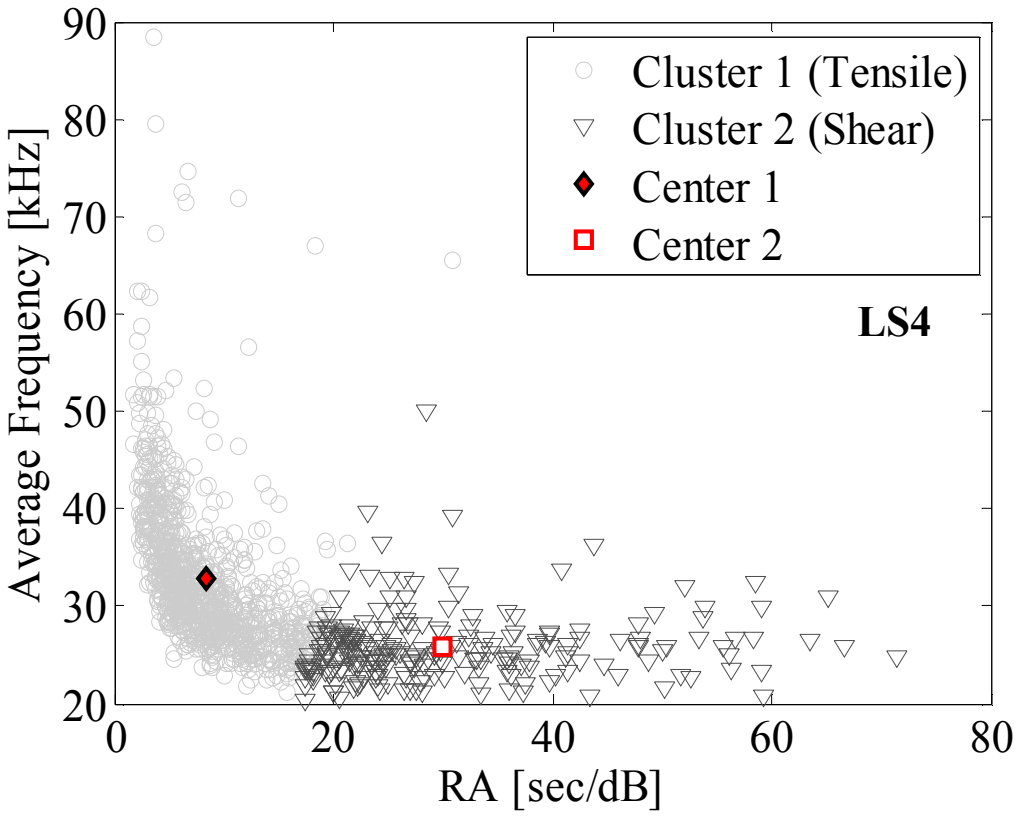

(a)

Figure 12. *k*-means analysis results in (a) LS4 and (b) LS5

Journal of Structural Engineering. Submitted May 4, 2012; accepted November 28, 2012;
posted ahead of print December 1, 2012. doi:10.1061/(ASCE)ST.1943-541X.0000781

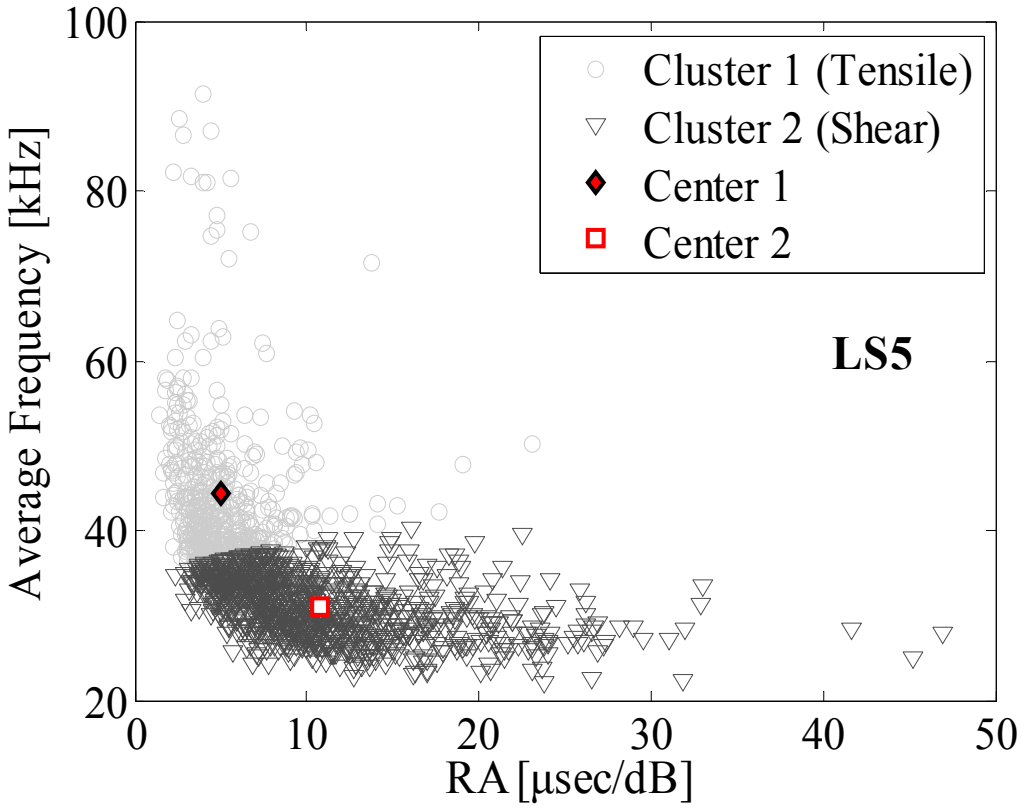

(b)

Figure 12. *k*-means analysis results in (a) LS4 and (b) LS5

Journal of Structural Engineering. Submitted May 4, 2012; accepted November 28, 2012;
posted ahead of print December 1, 2012. doi:10.1061/(ASCE)ST.1943-541X.0000781

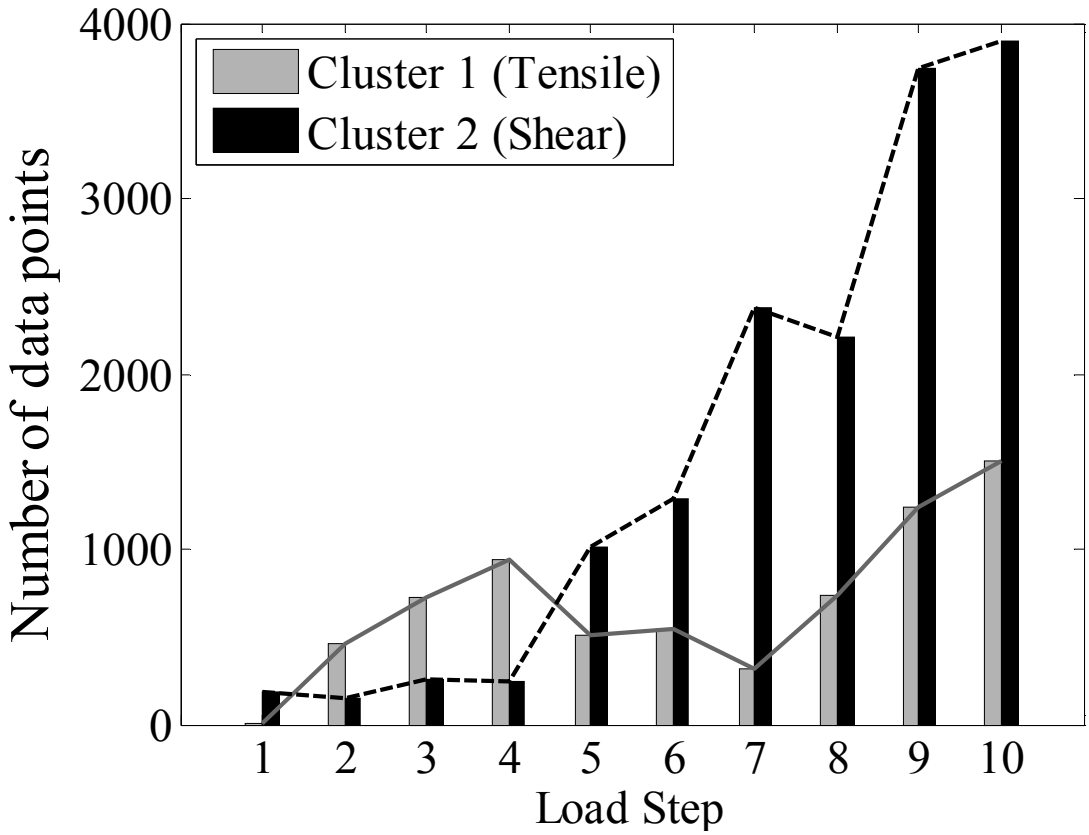

Figure 13. Number of data points associated to each cluster versus increasing load steps

Journal of Structural Engineering. Submitted May 4, 2012; accepted November 28, 2012;
posted ahead of print December 1, 2012. doi:10.1061/(ASCE)ST.1943-541X.0000781

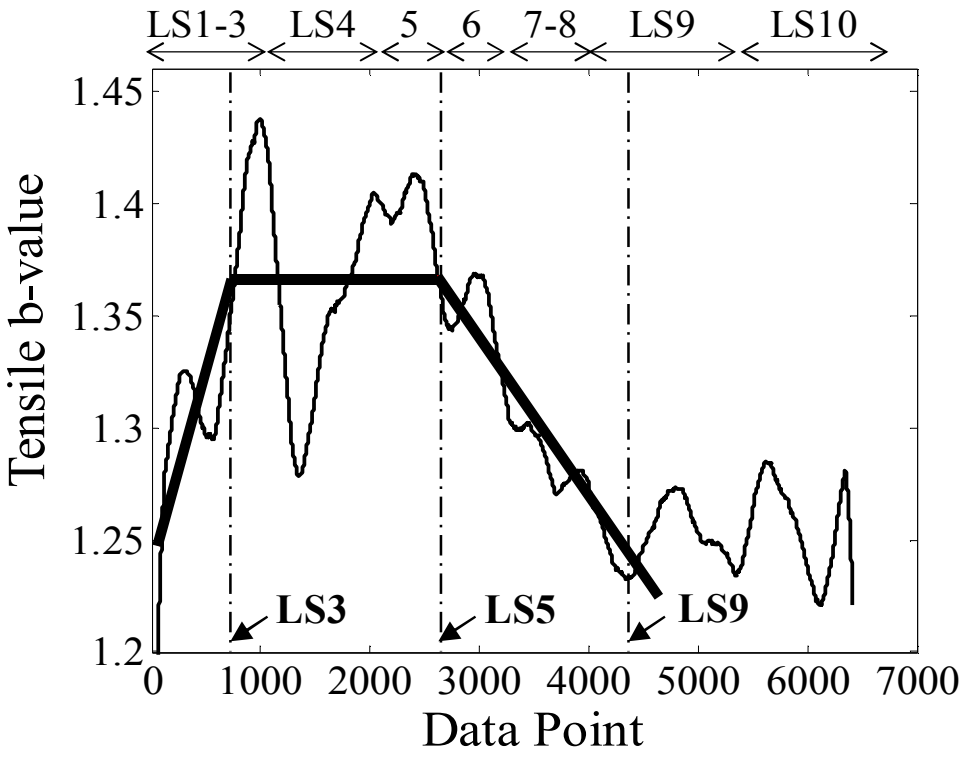

(a)

Figure 14. Sifted *b*-value analysis results: (a) Tensile class (b) Shear class

Journal of Structural Engineering. Submitted May 4, 2012; accepted November 28, 2012;
posted ahead of print December 1, 2012. doi:10.1061/(ASCE)ST.1943-541X.0000781

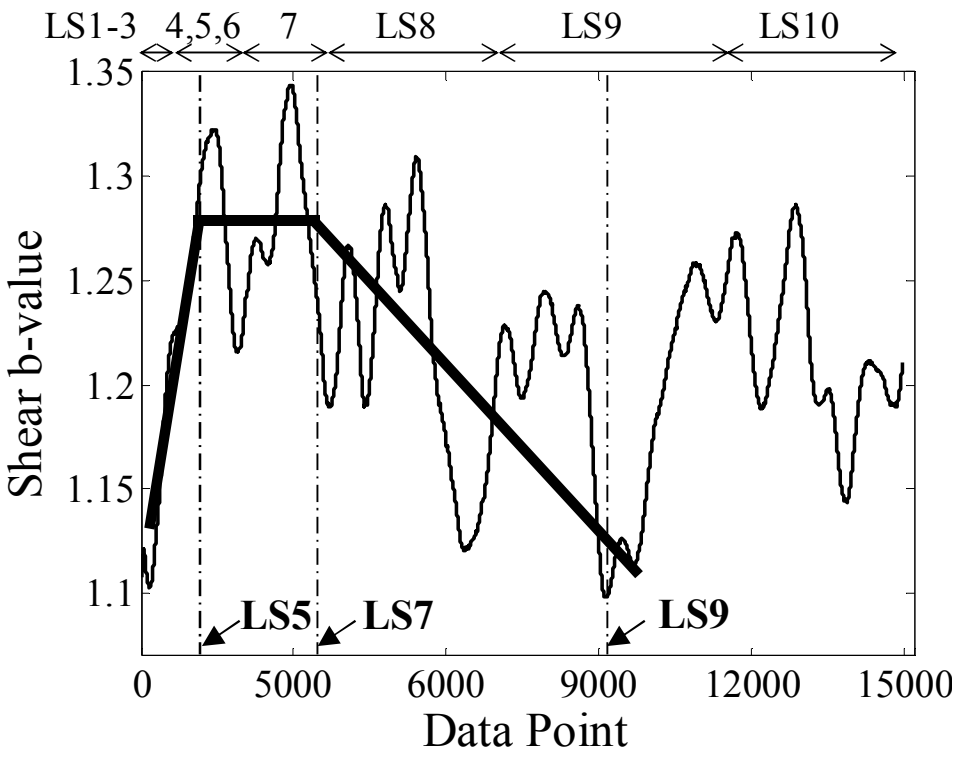

(b)

Figure 14. Sifted *b*-value analysis results: (a) Tensile class (b) Shear class